ACS OMEGA

http://pubs.acs.org/journal/acsodf

Article

Polyelectrolyte in Electric Field: Disparate Conformational Behavior along an Aminopolysaccharide Chain

Paween Mahinthichaichan, Cheng-Chieh Tsai, Gregory F. Payne, and Jana Shen*

Cite This: *ACS Omega* 2020, 5, 12016−12026

Read Online

ACCESS | Metrics & More | Article Recommendations | Supporting Information

ABSTRACT: Electrical signals are increasingly used in fabrication of hydrogels (e.g., based on aminopolysaccharide chitosan) to guide the emergence of complex and anisotropic structure; however, how an imposed electric field affects the polymer chain conformation and orientation during the self-assembly process is not understood. Here, we applied nonequilibrium all-atom molecular dynamics simulations to explore the response of a charged chitosan chain comprising 5- or 20-monomer units to a constant uniform electric field in water and salt solution. While no conformational or orientational response was observed for the polyelectrolyte (PE) chains under the small electric fields within the simulation time, a field strength of 400 mV/nm induced significant changes. In water, a 5-mer chain is found to be slightly bent and oriented parallel to the field; however, surprisingly, a 20-mer chain displays candy-cane-like conformations whereby one half of the chain is collapsed and flexible, while the other half of the chain is stretched along the electric field. In salt solution, the disparity remains between the two halves of the 20-mer chain, although the backbone is extremely flexible with multiple bent regions and non-native conformations occur near the chain center in one of the three trajectories. The disparate conformational response along the polyelectrolyte chain may be attributed to the balancing forces between chain dynamics, electric polarization, counterion binding, and hydrodynamic pressure as well as friction. These findings reconcile existing experiments and theoretical studies and represent an important step toward understanding the complex roles of electric field and salt in controlling the structure and properties of soft matter.

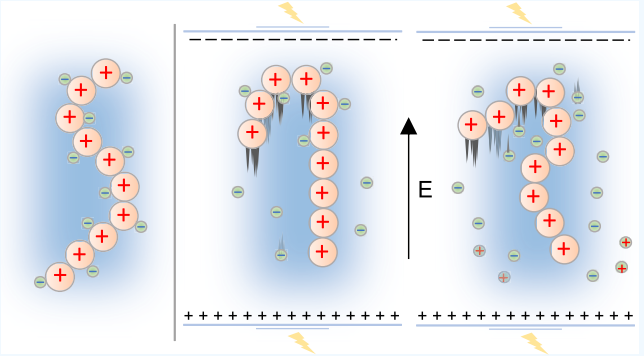

1. INTRODUCTION

Hydrogels are an important class of materials found in a wide range of applications, ranging from regenerative medicine to bioelectronics.[1] Over the past decade, many methods have been developed to fabricate hydrogels, e.g., printing and photolithographic approaches; however, these methods often lack the ability to controllably generate complex and anisotropic internal microstructures such as those characteristics of biological tissues, e.g., alignment of collagen fibers in the cornea.[2] Electrochemically based biofabrication methods have been recently reported,[2,3] in which external electrical signals are imposed to guide self-assembly. In several cases, the imposed electric field has been reported to offer control of the polymer chain conformation and orientation during the self-assembly process, e.g., for silk protein[4,5] and collagen,[6,7] and these observations suggest the broad potential of enlisting electric fields to control emergent structures. One challenge is however that the response of biopolymers to electric input is complex and poorly understood. The aminopolysaccharide chitosan is one of the best-studied examples of how an imposed electric field can guide the emergence of structure,[3,8−11] and yet even in this case, a detailed understanding of how electric field affects the polyelectrolyte (PE) in solution and guides the gelation process is lacking.

Derived from chitin, nature's second most abundant polymer, chitosan is made up of β-(1-4)-linked D-glucosamine monomer units (Figure 1). Under mildly acidic conditions, chitosan is soluble as a cationic polyelectrolytes (PEs), while at pH above 6.5,[12,13] glucosamines are neutralized and sol-to-gel transition occurs via intermolecular hydrogen bonds.[14] In recent years, a cathodic electrodeposition method to fabricate chitosan hydrogels[15−17] has been combined with temporary controlled electric signals to create complex internal patterns and multilayer structures.[3,18] It was hypothesized that electric field is responsible for recruiting soluble chitosan chains to the cathode−water interface and orienting them at the growing gel front to create patterns.[3] A recent molecular dynamics (MD)

Received: January 13, 2020
Accepted: May 11, 2020
Published: May 19, 2020

https://dx.doi.org/10.1021/acsomega.0c00164
ACS Omega 2020, 5, 12016−12026

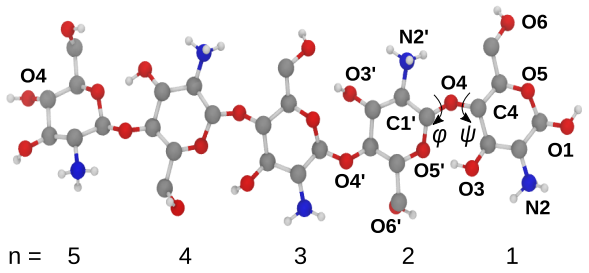

Figure 1. Structure of a fully charged 5-mer chitosan chain. Nonpolar hydrogen atoms are hidden for clarity. Atoms in monomer units 1 and 2 are labeled. The ϕ and ψ angles of the glycosidic linkage 2 (between monomers 1 and 2) are indicated.

study[3] demonstrated that a charged chitosan chain migrates in solution under a constant uniform (DC) electric field of 4 mV/nm and the migration speed is reduced by the addition of salt. However, how electric field affects the orientation and conformation of a chitosan chain, particularly in the presence of added salt, remains unclear.[3,19] Electric field strength and salt concentration are two important tunable parameters in electrobiofabrication methods.[2] Experiments suggested that salt modulates the mechanical property and internal structure of chitosan films,[3,20] and in a most recent study,[21] salt effect was exploited to make Janus films for bone regeneration. Atomically detailed understanding and quantitative predictions can rationalize experiments and guide the design to generate soft matter with controllable structure and properties.

The electric field-induced conformational effect on PEs remains a topic of debate. Scaling theories[22,23] and coarse-grained simulations[24] suggested that a collapsed polyelectrolyte chain in salt solution unfolds under an external electric field when the field strength reaches a critical value. However, field-induced PE stretching has not been conclusively demonstrated by experiments. While small electric fields do not perturb the conformation of a large DNA, a large alternating current (AC) electric field of 10 000 V/cm was suggested to induce stretching of DNA molecules by a microscopy experiment.[25] A more recent study using single-molecule fluorescence microscopy, however, showed that the bacterial phage T4 DNA becomes significantly more compact under a DC electric field and becomes a globule at a field strength of 250 V/cm or 2.5×10^{-2} mV/nm.[26] Similar observation was made in microfluidic experiments.[27] The collapse of λ-DNA was also observed under AC electric fields at sufficiently high strength using fluorescence microscopy,[28,29] and the authors suggested that the earlier observation of DNA stretching was due to an artifact of video microscopy. However, the authors also noted that when the field strength was further increased above 1220 V/cm or 0.122 mV/nm, the DNA appeared to elongate in the direction of electric field.[29]

The orientational effect of electric field on PEs is also under debate. Analytical theories[23,30] and coarse-grained simulations[23,31] predicted that a stiff PE is oriented parallel to the electric field, consistent with the evidence from experiments of rodlike single-stranded RNAs[32,33] and DNAs.[25,34] However, theoretical argument[30,35,36] and mesoscopic simulations[31] also suggested that hydrodynamic effect (solvent friction), which is in competition with the polarization mechanism, can result in bending for a flexible PE and/or orient it perpendicular to the field. The latter is supported by evidence from the birefringence experiment of poly(styrenesulfonate).[37]

All-atom molecular dynamics (MD) simulation in fully explicit solvent makes use of physics-based, empirically parameterized energy function (force field) to describe conformational dynamics of macromolecules with explicit representation of interactions between solute, solvent, and ions. As such, quantitative predictions of solution-phase macromolecular conformational dynamics can be made. Our recent MD study[38] showed that the persistence length of a single charged chitosan chain decreases from about 5.1 nm in pure water to about 2.8 nm in a solution of 0.5 M NaCl. Interestingly, the MD simulations revealed that in addition to the commonly known mechanism, i.e., screening of electrostatic repulsion between charged monomers, salt ions induce the chitosan chain collapse by disrupting an intramolecular hydrogen bond associated with the extended backbone conformations. Such atomic details cannot be obtained by analytical theories or coarse-grained simulations.

In this work, we performed nonequilibrium all-atom MD simulations of 5-mer and 20-mer charged chitosan chains in pure water and salt solution under a DC electric field of 4, 20, or 400 mV/nm. Simulations revealed that while all electric field strengths induce chain migration, only the large field of 400 mV/nm affects the chain conformation and orientation. Although the chitosan electrodeposition experiments were conducted under a much smaller field (4×10^{-4} mV/nm),[3] the use of a larger electric field was justified for two reasons. First, considering the manufacture-reported molecular weight of about 200 kDa, the degree of chitosan chain polymerization is about 1000, which effectively reduces the minimum field strength by 200 (relative to the 5-mer) or 50 times (relative to the 20-mer). Second, a small field may not produce a noticeable effect within the limited simulation time scale (100 ns to 1 μS). Thus, to accelerate the process of conformational and orientational changes, we tested a large field (400 mV/nm). Interestingly, this field strength is in agreement with those found to produce conformational changes of biological systems in previous nonequilibrium MD simulations.[39,40] Surprisingly, the orientational and conformational response of the 20-mer chain abruptly switches in the middle of the chain, which can be attributed to the balancing forces between PE chain dynamics, electric polarization, counterion binding, and hydrodynamic friction. Our findings reconcile current experiments and theoretical studies and have implications for electrofabrication of chitosan and other PE-based soft matter with complex and anisotropic structure.

2. RESULTS AND DISCUSSION

2.1. Conformation and Orientation of a 5-mer Chitosan Chain in Salt-Free Solution under Electric Fields. To investigate the field effects, a 5-mer charged chitosan chain was simulated in pure water with an applied DC electric field of 0, 4, 20, or 400 mV/nm (Table 1). While all field strengths (4−400 mV/nm) induce a center-of-mass translation of the chain in the direction of the electric field, i.e., toward the negative electrode, here we focus on the conformational and orientational effects. The probability distributions of the end-to-end distance (R_{ee}) from the small-field (4 and 20 mV/nm) and field-free simulations are similar (Figure 2a), suggesting that the small electric fields have a negligible effect on the chain dimension. By contrast, in the large-field (400 mV/nm) simulations, the most probable R_{ee} is decreased by about 0.5 nm and bent conformations (e.g., with

https://dx.doi.org/10.1021/acsomega.0c00164
ACS Omega 2020, 5, 12016−12026

Table 1. Overview of Molecular Dynamics Simulations of Two Charged Chitosan Chains in Pure Water and Salt Solutions at Different Electric Field Strengths

system	field (mV/nm)	salt (mM)	time (ns)
		5-mer Chain	
1	0	0	3 × 120
2	4	0	3 × 240
3	20	0	3 × 120
4	400	0	3 × 120
		20-mer Chain	
5	0	0	3 × 150
6	4	0	3 × 150
7	20	0	2 × 150
8	400	0	3 × 120 (150)[a]
9	0	500	3 × 150
10	4	500	3 × 150
11	20	500	2 × 150 (110)[b]
12	400	500	3 × 120 (150)[a]

[a]One of the simulations was run for 150 ns. [b]One of the simulations was run for 110 ns.

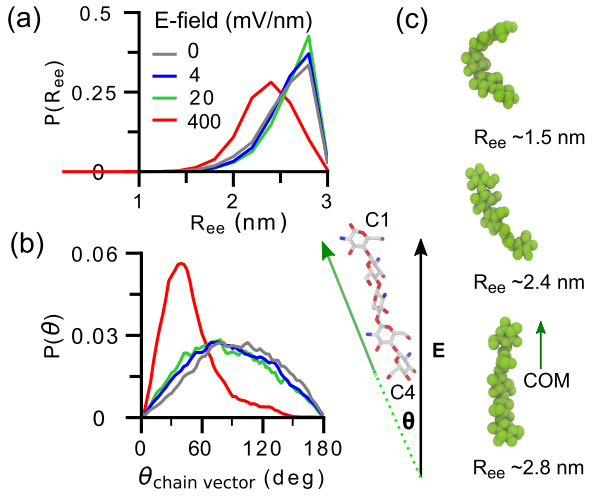

Figure 2. Conformation and orientation of a charged 5-mer chitosan in salt-free solution at different electric field strengths. (a) Probability distribution of the end-to-end distance R_{ee}, defined as the distance between O4 of the last and O1 of the first monomer unit. (b) Probability distribution of the angle (θ) between the chain vector and field direction. Data obtained at the electric field strengths of 0, 4, 20, and 400 mV/nm are shown in gray, blue, green, and red, respectively. At zero-field strength, the angles were calculated with respect to the z-direction. (c) Representative snapshots from the simulations at the field strength of 400 mV/nm. The direction of the center-of-mass movement of the chain is indicated by an arrow.

R_{ee} smaller than 2 nm) are more frequently sampled in the large field (Figure 2a), suggesting that the large electric field induces chain bending, as can be seen from the simulation snapshots (Figure 2c).

To examine the possible orientational effect of electric field, the probability distribution of the angle between the 5-mer chitosan chain vector (from the C4 atom of the last monomer to the C1 atom of the first monomer) and the electric field direction (Figure 2b) was calculated for simulations at different electric field strengths. Consistent with the end-to-end distance distributions, the chain vector angle distributions from the small-field and field-free simulations are similar, suggesting no particular preference. However, the distribution from the large-field simulations displays a sharp peak at about 35° (Figure 2b), suggesting that the 5-mer chain vector is oriented nearly parallel to the electric field (Figure 2c).

2.2. Comparison to Experiments and Theories of PE Orientation in Electric Field. The orientational preference of the 5-mer chitosan chain is consistent with the birefringence measurements of rodlike single-stranded RNAs[32,33] and charged micelles[41] as well as dichroism and fluorescence microscopy of DNAs,[25,34] which suggested that a charged stiff PE orients parallel to an applied electric field in dilute solutions. The parallel orientation is also in agreement with several theoretical studies and coarse-grained simulations,[22,23,35,42] which suggest that the induced dipole of a rigid PE under an external field arises from the deformation of the counterion cloud along the PE chain. We will come back to counterion binding in a later part of the paper.

2.3. Extended Syn Conformation Is Less Sampled by the 5-mer Chain under the Large Electric Field. Our previous work[38] demonstrated that the rigidity of a short chitosan chain, such as the 5-mer, which has a contour length below the persistent length, can be explained at the microscopic level by the dominant sampling of the extended glycosidic backbone conformations known as the syn state, in which the glycosidic linkage angle (C1′−O4−C4, see Figure 1) fluctuates around 150°.[38] By contrast, bent conformations or turns are associated with the anti-ψ and anti-ϕ states, in which the glycosidic linkage angle fluctuates around 115 and 125°, respectively.[38] Thus, we hypothesized that the electric field may induce a population shift from syn to anti states. To test the hypothesis, we calculated the free-energy surfaces of ϕ (H1′−C1′−O4−C4) and ψ (C1′−O4−C4−H4) torsion angles of the four individual glycosidic linkages in the 5-mer chain (Figure 3).

In the field-free simulations, the (ϕ, ψ) free-energy maps of glycosidic linkages display a global minimum in the region centered around (45, −40°), corresponding to the syn state (Figure 3a, top). In the syn conformations, the two adjacent sugar rings are in plane with the amino groups on the opposite sides of the rings (Figure 3b, top). By contrast, a local minimum in the (ϕ, ψ) map is located in the region, where ψ is above 90° or below −100°, corresponding to the anti-ψ state (Figure 3a, top). In the anti-ψ conformations, two adjacent sugar rings are perpendicular to each other (Figure 3b, middle). Finally, a minor minimum in the (ϕ, ψ) map can be found where ϕ is above 125° or below −100°, corresponding to the anti-ϕ state (Figure 3a). In the anti-ϕ conformations, which are seldom sampled by a chitosan chain, two adjacent sugar rings are in-plane but the amino groups are on the same side of the sugar rings (Figure 3b, bottom).

We examine the (ϕ, ψ) maps of the individual glycosidic linkages in the 5-mer chitosan from simulations at different electric field strengths. Simulations in the small fields (2, 40 mV/nm) resulted in similar maps as the field-free ones; however, the maps from the large-field simulations show destabilization of the syn region and stabilization of the anti-ψ and to a smaller extent also the anti-ϕ regions (Figure 3a, bottom). We calculated the percentage populations of the syn, anti-ψ, and anti-ϕ states for the individual glycosidic linkages. Consistent with the (ϕ, ψ) maps, the percentage populations of the three states from the small-field simulations are similar to the field-free simulations (Figure 3b). However, in the large-field simulations, the syn population is decreased by more than 30% and the anti-ψ population is increased by more than 20%

https://dx.doi.org/10.1021/acsomega.0c00164
ACS Omega 2020, 5, 12016−12026

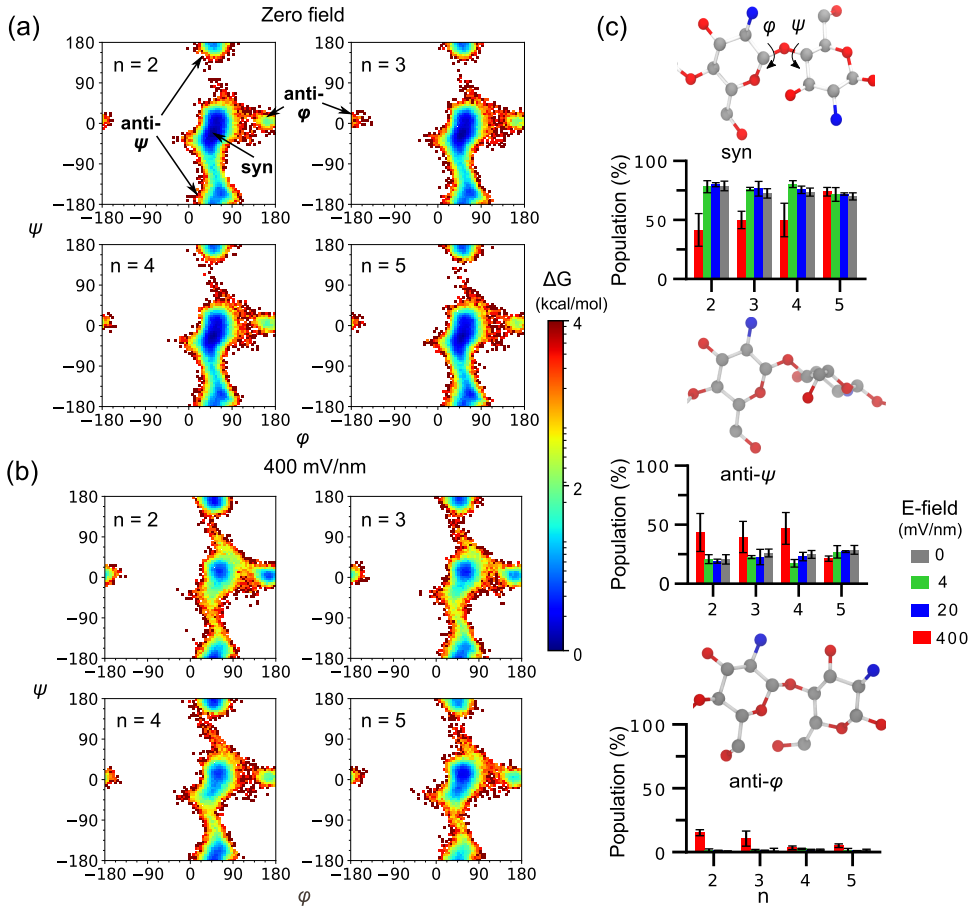

Figure 3. Glycosidic conformations of a charged 5-mer chitosan in pure water at different electric field strengths. The free-energy (ΔG) maps as a function of (ϕ, ψ) angles for the individual glycosidic linkages in the 5-mer chitosan from the field-free simulations (a) and simulations at the field strength of 400 mV/nm (b). ΔG was calculated as $-kT \ln P(\phi,\psi)$, where P is the probability of finding the dihedral angles in a particular bin, k is the Boltzmann constant, and T is the temperature, 300 K. (c) Structures and percentage populations of syn (top), anti-ψ (middle), and anti-ϕ (bottom) states for the individual glycosidic linkages in the 5-mer chain. Following our previous work,[38] the syn state is defined as $-90° \leq \phi \leq 125°$ and $-100° \leq \psi \leq 90°$, the anti-ϕ state is defined as $\phi > 125$ or $<-100°$, and the anti-ψ state is defined as $\psi > 90$ or <-100 °. The error bar represents the root-mean-square fluctuation in the simulations.

for the first three glycosidic linkages (Figure 3b). There is also a 10−15% increase in the anti-ϕ population for the first two glycosidic linkages (Figure 3b). Interestingly, the percentage populations of the last glycosidic linkage (monomers 4 and 5) remain similar to the field-free values. Since the syn state is associated with the extended backbone and the anti-ψ state is associated with the bent backbone and turns, the population shift from the syn to anti-ψ state offers a microscopic explanation for the field-induced chain bending.

2.4. 20-mer Chitosan Chain Samples the Candy-Cane-like Conformations in Salt-Free Solution under the Large Electric Field. Having found that a large electric field induces slight bending and parallel orientation for a rigid 5-mer chitosan, we proceeded to explore the field effects on a 20-mer chitosan, which has been demonstrated as semiflexible in the field-free simulations.[38] Simulations were performed at the electric field strengths of 4, 20, and 400 mV/nm (Table 1), and all of them induced chain migration toward the negative electrode, whereby the speed increases with the field strength as expected (Figure S1). Similar to the 5-mer chitosan, smaller electric fields do not perturb the chain dimension; however, in the large electric field, the 20-mer chain is significantly collapsed. Surprisingly, the collapse only occurs in monomers 1−10, while monomers 11−20 are fully stretched (see snapshots in Figure 4a). The time series of the end-to-end distances demonstrate that the collapse of monomers 1−10 appeared within the first 30 ns and subsequently the chain dimension remained stable throughout the simulation runs (Figure S2). The most probable end-to-end distance of monomers 1−10 is reduced by about 3 nm compared to the field-free value (Figure 4b, top); however, the most probable end-to-end distance of monomers 11−20 is similar to the contour length and nearly 1 nm larger than the field-free value (Figure 4b, bottom). These data demonstrate a surprising conformational disparity between the two halves of the chitosan chain. Due to the collapse of the first 10 monomers, the overall chain dimension is significantly reduced (Figures S3 and S4).

2.5. Comparison to Experiments and Theories of PE Chain Conformations in Electric Field. Single-molecule fluorescence microscopy[26] and microfluidic experiments[27] demonstrated that DNAs become compact under large electric fields. The backbone bending showed by our simulations of the 5-mer and 20-mer chitosan chains is consistent with these experiments. Interestingly, the conformations of the 5-mer and 20-mer chains from our simulations are reminiscent of the conformational transitions of short actin filaments in simple shear flow.[43] Fluorescence imaging data showed that as the

https://dx.doi.org/10.1021/acsomega.0c00164
ACS Omega 2020, 5, 12016−12026

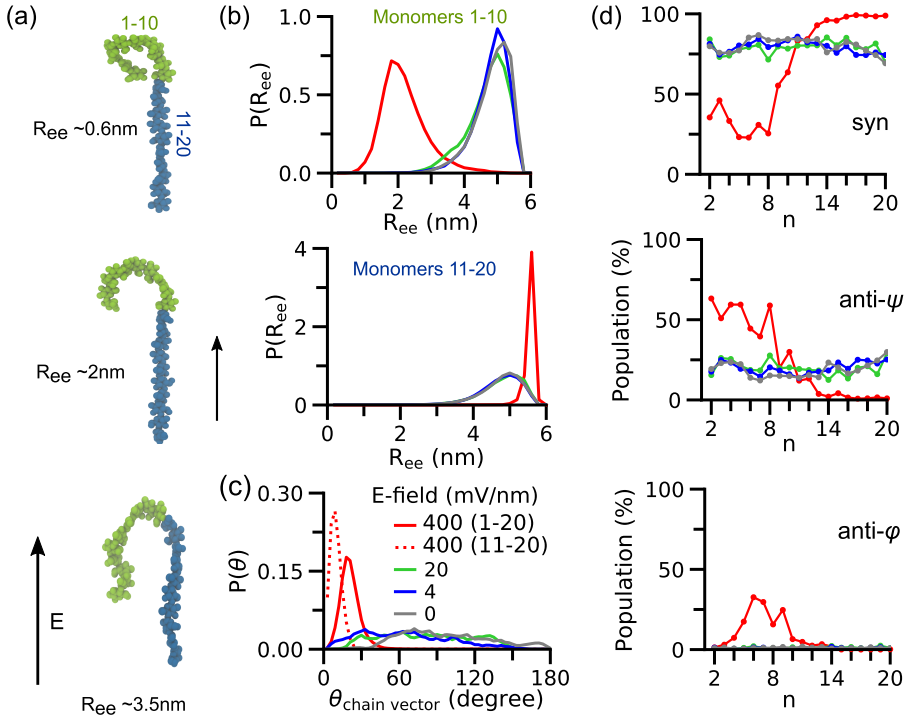

Figure 4. Conformation and orientation of a charged 20-mer chitosan chain in salt-free solution at different electric field strengths. (a) Snapshots from the simulations in the large electric field with monomers 1−10 and 11−20 colored in yellowish-green and blue, respectively. The directions of the electric field and the center-of-mass movement are indicated by arrows. The shown R_{ee} values correspond to those of monomers 1−10. (b) Probability distributions of the end-to-end distance of the first half (monomers 1−10, top) and second half of the chain (monomers 11−20, bottom). (c) Probability distribution of the angle of the chain vector with respect to the direction of electric field. The chain vector is defined as C4 of the last to the C1 atom of the first monomer unit (or monomer unit 11 in the dashed curve). At zero field, the angle with respect to z was used. (d) Percentage populations of the syn, anti-ϕ, and anti-ψ states for the individual glycosidic linkages (n) in the chain.

ratio between the contour and persistence length of the filament increased to 0.34, a transition from stiff filament tumbling to "global buckling" (chain bending) occurred and a further increase of the ratio to 1.2 led to J shape and U turns.[43]

According to the macroscopic scaling theory of Netz,[22,23] a charged 20-mer chitosan should stretch out in an electric field larger than 2 mV/nm (see Section 4.3). However, our simulations showed that while one half of the chain is stretched, the second half of the chain is collapsed. We attribute the discrepancy to the neglect of hydrodynamic effects in the theory.[22,23] In fact, using fluid mechanics simulations of an elastic rodlike PE moving in an electric field, Netz and co-workers showed that the PE is bent to a U-like shape, whereby the curved part is oriented perpendicular to the direction of motion and the opening points backward.[35,36] They reasoned that the effective force pushing the rod is larger in the middle, because the middle receives hydrodynamic thrust from both sides of neighboring segments.[35,36] Similarly, hydrodynamic forces were also suggested as the reason for buckling and strongly bent conformations of actin filaments in simple shear flow.[43] We suggest that the hydrodynamic mechanism underlies the observed bending of the chitosan chains in the large electric field.

2.6. 20-mer Chitosan Is Oriented along the Electric Field in Salt-Free Solution. To examine the electric field effect on the orientation of the 20-mer chain in pure water, we calculated the distributions of the chain vector angle from the simulations at different field strengths (Figure 4c). Under the small electric fields, the distributions are identical to the field-free one, suggesting that the small electric fields do not perturb the chain orientation. However, under the large electric field, the distribution for the entire chain vector displays a peak around 30°, while the distribution for monomers 11−20 displays a sharp peak at 0°, indicating that the fully extended part of the chain is perfectly aligned with the field (Figure 4a). Snapshots show that the 20-mer chitosan moves toward the negative electrode with the curved part oriented perpendicular and the straight part oriented parallel to the field line (Figure 4a).

2.7. Candy-Cane-like Conformations Arise from the Disparate Syn Populations. The (ϕ, ψ) free-energy maps for the glycosidic linkages of monomers 1−10 reveal significant destabilization of the syn and stabilization of the anti-ψ, anti-ϕ, and syn-to-anti-ψ transition regions (Figure S5). These changes result in a decrease of the syn population to below 40% and increase of the anti-ψ and anti-ϕ populations to about 60 and 15−35%, respectively (Figure 4d). Remarkably, the conformational behavior abruptly switches in the middle of the 20-mer chain, at the glycosidic linkage between monomers 10 and 11. The (ϕ, ψ) maps of the glycosidic linkages of monomers 11−20 show stabilization of the syn region exclusively (Figure S5). As a result, the syn population is increased to nearly 100% and the anti-ψ and anti-ϕ populations vanish (Figure 4d), consistent with the full extension of monomers 11−20.

2.8. Conformational Effect of the Large Electric Field Is Different in Salt Solution. The small electric fields have no effect on the 20-mer chitosan chain in a 0.5 M NaCl solution. The distributions of the end-to-end distance and radius of gyration of the 20-mer chain from the small-field

https://dx.doi.org/10.1021/acsomega.0c00164
ACS Omega 2020, 5, 12016−12026

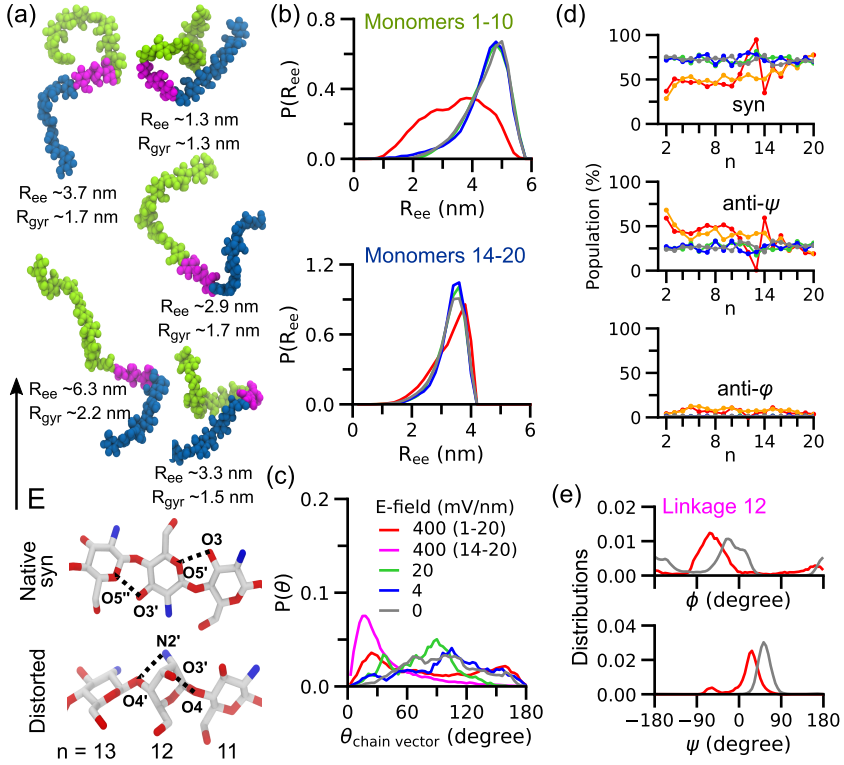

Figure 5. Conformation and orientation of the 20-mer charged chitosan chain in a 0.5 M NaCl solution at different electric field strengths. (a) Snapshots from the simulations in the large electric field with monomers 1−10, 11−13, and 14−20 colored in yellowish-green, magenta, and blue, respectively. Snapshots of the native syn and distorted conformations of monomers 11−13 (taken from one of the three large-field simulations) are displayed at the bottom. The non-native hydrogen bonds are shown in dashed lines. (b) Probability distribution of the end-to-end distance of monomers 1−10 (top) and monomers 14−20 (bottom) at different field strengths. The end-to-end distance refers to that between O1 of the first and O4 of the last monomer units. (c) Probability distribution of the chain vector angle with respect to the field direction. Magenta data refers to monomers 14−20. (d) Percentage populations of the syn, anti-ϕ, and anti-ψ states for the individual glycosidic linkages (n). Note, in one of the large-field simulations, non-native conformations were observed (red). Such conformations did not occur in the other two simulations (orange). (e) Probability distributions of ϕ (top) and ψ (bottom) angles of the glycosidic linkage 12 in zero-field (gray) and one of the large-field simulations (red).

simulations remain similar to those from the field-free simulations (Figure S3). However, in the large-field simulations, the end-to-end distance and radius of gyration of the 20-mer chain are significantly reduced (Figures S3 and 5a). Interestingly, unlike in pure water, the large electric field did not produce candy-cane-like conformations with a single dominant bending region. Instead, simulation snapshots show conformations with multiple bending regions (Figure 5a). The significant increase in chain flexibility and loss of order in the presence of added salt is consistent with the observation that the electrodeposited chitosan hydrogel has lower moduli[20] and minimal birefringence (i.e., minimal chain alignment).[3] In some of the compact conformations, the two chitosan chain tails cross each other, suggesting the possibility of forming self-entangled states given a longer chain length (i.e., a higher degree of polymerization). Electric field-induced self-entanglement and knotting have been observed for DNAs in fluorescence microscopy[26] and solid-state nanopore experiments.[44] The field-induced bending and increase in the backbone flexibility revealed by our simulations are consistent with these observations.

For monomers 1−10, the most probable end-to-end distance is decreased by 1−1.5 nm relative to the field-free value and the chain flexibility is significantly increased, as demonstrated by a significant reduction in the peak height of the end-to-end distance distribution (Figure 5b, top). What about the second half of the 20-mer chain, monomers 11−20? Surprisingly, the large electric field induces a backbone distortion for monomers 11−13 (Figure 5a), while the end-to-end distance distribution for monomers 14−20 remains similar to the field-free one (Figure 5b, bottom). Thus, unlike in pure water, the large electric field does not stretch out the backbone of monomers 14−20, which remains somewhat collapsed and flexible due to added salt. However, similar to the behavior in pure water, this part of the chain is oriented nearly parallel to the electric field, as demonstrated by a sharp peak at about 25° in the angle distribution for the chain vector spanning monomers 14−20 (Figure 5c).

2.9. Large Electric Field Can Induce Non-native Backbone Conformations in Salt Solution. We next examine the glycosidic backbone conformations. Under the large field, a population shift from the extended syn to the bent anti-ψ state is observed for the glycosidic linkages of monomers 1−10 in 0.5 M NaCl solution, similar to the effect in pure water (Figure 5d). In contrast, monomers 14−20 sample a similar amount of syn conformations as in the field-free simulations (Figure 5d), consistent with the negligible effect of the field on the end-to-end distance (Figure 5b, bottom). Surprisingly, a significant change in the backbone conformation near the middle of the 20-mer chain (from monomer 11 to 13) occurred within 10 ns and remained stable throughout one of the three simulation runs (Figures S6 and

https://dx.doi.org/10.1021/acsomega.0c00164
ACS Omega 2020, 5, 12016−12026

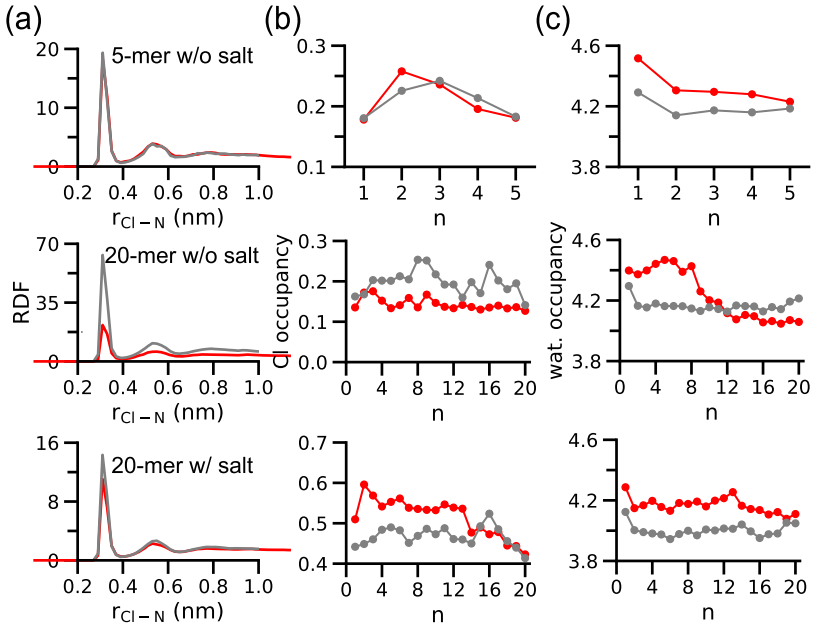

Figure 6. Electric field effect on the counterion distribution around the 5-mer and 20-mer chitosan chains. (a) Radial distribution function, RDF, profiles of chlorides around the amine nitrogens of the 5-mer chain (top), 20-mer chain in salt-free solution (middle), and 20-mer chain in 0.5 M NaCl solution (bottom). The gray and red lines correspond to the electric field strengths of 0 and 400 mV/nm, respectively. (b) Occupancies of directly bound chloride ions to the individual amines of the 5-mer in water (top), 20-mer in water (middle), and 20-mer chain in 0.5 M NaCl solution (bottom). An ion is considered bound if its distance to the amine nitrogen is within 0.4 nm (first minimum in the RDF profile). (c) Occupancies of directly bound water to the individual amines of the 5-mer in water (top), 20-mer in water (middle), and 20-mer chain in 0.5 M NaCl solution (bottom). A water is considered bound if its oxygen to amine nitrogen distance is within 0.35 nm (first minimum in the RDF profile). Occupancy is represented by the root-mean-square number $\sqrt{\langle N^2 \rangle}$ of ions or water.

S7). The distributions of the ϕ and ψ angles of glycosidic linkage 12 show that the major peaks are left-shifted compared to the field-free simulations by nearly 40° (Figure 5e). Similar distributions of glycosidic linkage 13 also demonstrate changes (Figures S8 and S9). Snapshots revealed that the O4 atom of monomer 11 forms a hydrogen bond with the O3 atom of monomer 12, while the N2 atom of monomer 12 forms a hydrogen bond with the glycosidic O4 atom (Figure 5a, bottom). These data demonstrate that the large electric field-induced non-native conformations are stabilized by non-native hydrogen bonds. Given that this behavior was only observed in one of the three trajectories, we suggest that it may be a kinetically trapped state.

2.10. Why Does Electric Field Produce Disparate Behavior along the Chitosan Chain? To understand the electric field effects on PEs, we need to consider the polarization of the counterion atmosphere. We calculated the radial distribution functions (RDFs) of chloride ions around amine nitrogens as well as the occupancies of directly bound or condensed chloride ions for the 5-mer and 20-mer chitosan chains in simulations at the field strengths of 0 and 400 mV/nm (Figure 6). Note, the data for small fields are not shown as the effects are negligible.

For the 5-mer chain, the total number of chlorides that are directly bound (first peak in the RDF) and those forming water-mediated interactions (second peak in the RDF) is similar in the field-free and large-field simulations (Figure 6a, top). However, the spatial distribution of ions is changed in the large electric field. In contrast to the symmetric ion distribution at zero-field strength, i.e., the middle of the chain has somewhat higher occupancy of ions compared to the ends, the occupancy of ions is somewhat increased at monomer 2 and decreased at monomers 3 and 4 under the large electric field (Figure 6b, top). This data indicates that the ion cloud is polarized by the electric field. The deformation of the ion cloud due to anisotropic electric polarization has been theoretically argued to favor the parallel orientation of a PE chain.[35,36]

For the 20-mer chitosan chain in pure water, the total number of directly bound and solvent-mediated chloride ions is significantly reduced in the large-field simulations compared to the field-free simulations (Figure 6a, middle). With added salt, the field-induced reduction in counterion binding is also seen, albeit to a much smaller extend (Figure 6a, bottom). These data indicate that the counterions are stripped away from the chitosan chain, which can be attributed to the electric forces on the ions. It is not surprising that such an effect is less pronounced in salt solution, due to the presence of a large number of salt ions.

Turning to the counterion occupancy at individual monomer sites, we can see that in pure water, the ion occupancy is reduced everywhere (Figure 6b, middle); however, in salt solution, a significant reduction is only seen at monomers 14−20 (Figure 6b, bottom). Nonetheless, consistent with the trend seen for the 5-mer chain under the large electric field (Figure 6b, top), the ion occupancy appears to be lower at monomers 11−20 in pure water or 14−20 in salt solution as compared to monomers 1−10. The reduction and polarization of counterion atmosphere in a large electric field observed here are consistent with the result from an early study of rodlike PEs using coarse-grained Monte Carlo simulations.[42]

To investigate the hydrodynamic effect under the large field, we calculated the hydration number of individual amines along the chitosan chain (Figure 6c). In the absence of salt, the

https://dx.doi.org/10.1021/acsomega.0c00164
ACS Omega 2020, 5, 12016−12026

number of water surrounding the individual amine units in the collapsed first half of the 20-mer chain is significantly larger than that surrounding the amines in the extended second half of the 20-mer chain (Figure 6c, middle), consistent with the hydrodynamic pressure acting on the first half of the chain, which is the moving front. In the presence of salt, the hydration of all amine of the 20-mer chain is increased relative to that in the field-free simulation. A sharp increase is observed at the monomer units 12 and 13 (Figure 6c, bottom), where a backbone distortion occurs, attributable to the hydrodynamic shear force.

Our previous work showed that the presence of salt ions induces chitosan chain collapse and increased flexibility via two mechanisms: (1) disruption of the O3···O5′ hydrogen bond, which stabilizes the extended syn conformations, and (2) weakening of the electrostatic repulsion between charged glucosamine units. Therefore, a reduction in counterion binding would decrease the above effect, leading to chain straightening and increased stiffness. This explains why the part of the chain that has a larger reduction in counterion binding due to the electric field is more extended, i.e., monomers 11−20 in simulations without salt (or monomers 14−20 in simulations with salt) are more extended compared to monomers 1−10. Thus, we suggest that the dramatic difference in the conformational behavior of the two halves of the chain can be attributed to the difference in counterion binding. The neglect of anisotropic polarization of counterion atmosphere may be the reason why previous continuum[22,23] and coarse-grained[24] simulations, in which counterion binding is uniformly reduced in electric field, predicted an overall chain stretching.

3. CONCLUSIONS

We have applied nonequilibrium all-atom molecular dynamics simulations to investigate the conformational and orientational changes of cationic chitosan chains under a DC electric field of 4, 20, or 400 mV/nm. The effects were negligible in the small fields of 4 and 20 mV/nm; however, the large field of 400 mV/nm induced significant conformational change and orientational preference for both the 5-mer and 20-mer chitosan chains. Interestingly, this field strength is in agreement with the field strength (100−500 mV/nm) found to cause conformational changes of biological systems in previous nonequilibrium MD simulations.[39,40] The 5-mer chitosan, which has the contour length half of the persistence length, is slightly bent and oriented nearly parallel to the electric field, which is also the direction of the center-of-mass movement. In pure water, the 20-mer chitosan, which has a contour length twice of the persistence length, displays candy-cane-like conformations, whereby the moving front part of the chain (monomers 1−10) is bent and flexible but the tail part (monomers 11−20) of the chain is extended, stiff, and oriented parallel to the field. We suggest that the disparate conformational behavior can be attributed to the difference in the field-induced reduction in counterion binding, in addition to the hydrodynamic effect, which causes chain bending. As compared to monomers 1−10, more counterions are tripped away from monomers 11 to 20, effectively increasing the electrostatic repulsion between charged monomers and contributing to chain extension.

Our findings explain the discrepancies between experiments and theories/coarse-grained simulations. Our simulations showed that the overall dimension of the chitosan chains is reduced by the large electric field, consistent with the experimental observations of DNA compaction under the electric field.[26−29] Our simulations revealed that the bending of the 20-mer chitosan chain occurs in the middle and the curved part is facing and perpendicular to the chain moving direction, which is in agreement with the hydrodynamic theory and simulations.[30,31,35,36] The chain stretching found in our simulations is in partial agreement with the macroscopic theory[22,23] and coarse-grained simulations,[24] which predicted overall chain stretching, as hydrodynamic effect and anisotropic counterion binding were neglected.

In salt solution, the 20-mer chitosan chain becomes more compact and not well aligned under the large electric field, consistent with the experimental observation of lower elastic modulus and minimal chain alignment in the electrodeposited chitosan hydrogel.[3,20] The effect of salt-induced chain collapse[38] competes with the field-induced chain stretching. As a result, monomers 14−20 are more extended than monomers 1−10 but not fully stretched as in salt-free solution. In one of the three independent simulation trajectories, the large electric field also distorts the backbone conformations of monomers 11−13 (glycosidic linkages 12 and 13), which likely represents a kinetically trapped state. Consistent with our previous finding that salt disrupts the native O3···O5′ hydrogen bond responsible for the extended syn state of the chitosan chain,[38] the backbone distortion is enabled by the breakage of the native and formation of a non-native hydrogen bond.

Taken together, the all-atom simulations offered a detailed view of the conformational and orientational response of the cationic chitosan to electric field. By explicitly describing the balancing forces between PE chain dynamics, electric polarization, counterion condensation, and hydrodynamic friction, our results captured the complex effects of electric field and resolved the long-standing controversy regarding the conformational response of PEs to electric field. A quantitative understanding of competing physical phenomena is essential to controlling the emergence of the structure.[45,46] Our work represents an important step toward understanding the complex roles of electric field and salt in controlling the structure and properties of soft matter.

4. METHODS AND PROTOCOLS

4.1. System Preparation. All-atom molecular dynamics simulations of chitosan chains in solution were performed using the GROMACS program (version 5.0).[47] The chitosan chains that were investigated are the 5-mer chain, comprising 5 charged glucosamine units, and the 20-mer chain, comprising 20 charged glucosamine units. The chitosan chains were represented by the CHARMM36 carbohydrate force field[48−50] and water was represented by the CHARMM-style TIP3P model.[51] To construct the initial simulation system, a fully extended chitosan chain was solvated in an octahedron water box with a minimum distance of 10 Å between the solute heavy atoms and the edge of the box. For the 5-mer chain, 5 chloride ions were added to neutralize the charge and the system contained 3598 water molecules. For the 20-mer chain, two systems were prepared. In the system with no added salt, 20 chloride ions and 52 524 water molecules were added. In the system with 0.5 M NaCl, additional 465 sodium and chloride ions were added by randomly replacing a solvent molecule with a sodium or a chloride ion.

4.2. Simulation Protocol. Following energy minimization to remove energetically unfavorable contacts, the system was

https://dx.doi.org/10.1021/acsomega.0c00164
ACS Omega 2020, 5, 12016−12026

equilibrated under constant NVT conditions for 100 ps and the temperature was maintained at 300 K by the Nosé–Hoover thermostat[52] using a time constant of 0.1 ps. Next, the system was equilibrated under constant NPT conditions for 100 ps, where the pressure was maintained at 1 atm using the isotropic Parrinello–Rahman pressure coupling method[53] with a time constant of 2.0 ps and compressibility of 4.5×10^{-5} bar^{-1}. During the minimization and equilibration, the heavy atoms of the chitosan chain were restrained with a harmonic force constant of 1000 kJ/(mol nm^2). Finally, a 150 ns unrestrained production run was performed under the constant NPT conditions and an external electric field at a temperature of 300 K and pressure of 1 atm. For the electric field strengths of 0, 4, and 20 mV/nm, three independent runs were performed starting from different random velocity seeds. The direction of the applied electric field was different in the three runs, i.e., x, y, or z. For the electric field strength of 400 mV/nm, three simulation runs were performed and the direction of the field was about 60° with respect to x. During molecular dynamics simulations, bonds involving hydrogens were constrained using the LINCS algorithm[54] to enable a 2 fs time step. The van der Waals interactions were smoothly switched to zero from 10 to 12 Å. The particle mesh Ewald method[55] was used to calculate long-range electrostatic energies with a sixth-order interpolation and 1 Å grid spacing.

4.3. Macroscopic Theory. In the macroscopic theory of PEs, the ratio of the Coulomb repulsion between PE monomers and thermal energy is described by a parameter called Coulomb interaction strength[31] or coupling parameter,[23] $\Xi = q^2 l_B/a$. Here, q is the charge valency of the PE monomers and l_B/a is commonly known as the normalized charge density, where l_B is the Bjerrum length (about 0.71 nm at room temperature in water), which describes the distance at which the electrostatic interaction between two elementary charges is comparable to thermal energy, and a is the radius of the PE monomer bead. For chitosan, q is 1 and a is roughly 0.28 nm.[38] Therefore, the coupling parameter Ξ for chitosan is about 2.5.

By comparing the polarization energy of PE and its counterions under an external electric field with thermal energy, Netz developed a scaling theory, which predicts that a collapsed PE chain stretches out in the direction of the field when the field strength is above a critical value[23]

$$E^* = \left(\frac{kT}{ae}\right)\left(\frac{N\Xi}{N_c}\right)^{1/2}\left(\frac{1}{l_p}\right)^{3(1-\nu)/2} N^{-3\nu/2} \quad (1)$$

where e is the elementary charge, N is the number of monomer units, N_c is the number of condensed counterions, l_p is the persistence length of the PE, and ν is the swelling exponent, which varies from 1 (rigid rodlike phase at extremely low-salt conditions) to 1/3 (collapsed phase at high-salt conditions).

From our previous work,[38] l_p of a charged chitosan chain is estimated to be 5.1 nm in pure water and 2.8 nm in 0.5 M NaCl solution. From the present simulations, N_c/N is estimated to be 0.6. Thus, for a charged 20-mer chitosan chain, eq 1 returns a critical field strength of 2.1 mV/nm in pure water and 4.2 mV/nm in salt solution.

■ ASSOCIATED CONTENT

Supporting Information

The Supporting Information is available free of charge at https://pubs.acs.org/doi/10.1021/acsomega.0c00164.

Convergence and additional conformational analyses; cumulative displacements of the 20-mer chitosan chain; conformations of the 20-mer chitosan chain; electric field effect; free-energy surface; free-energy map; percentage populations; stability of the distorted unit; probability distributions (Figures S1–S9) (PDF)

■ AUTHOR INFORMATION

Corresponding Author

Jana Shen − *Department of Pharmaceutical Sciences, University of Maryland School of Pharmacy, Baltimore, Maryland 21201, United States*; Email: jana.shen@rx.umaryland.edu

Authors

‖**Paween Mahinthichaichan** − *Department of Pharmaceutical Sciences, University of Maryland School of Pharmacy, Baltimore, Maryland 21201, United States*; orcid.org/0000-0002-2216-4482

‖**Cheng-Chieh Tsai** − *Department of Pharmaceutical Sciences, University of Maryland School of Pharmacy, Baltimore, Maryland 21201, United States*; orcid.org/0000-0002-7140-2766

Gregory F. Payne − *Institute for Bioscience and Biotechnology Research, University of Maryland, College Park, Massachusetts 20742, United States*; orcid.org/0000-0002-3234-0769

Complete contact information is available at: https://pubs.acs.org/10.1021/acsomega.0c00164

Notes

The authors declare no competing financial interest.

‖P.M. and C.-C.T.: Joint first authors.

■ ACKNOWLEDGMENTS

The authors thank the National Science Foundation (CBET1435957 and CBET1932963 to G.F.P. and J.S.) for funding.

■ REFERENCES

(1) Zhang, Y. S.; Khademhosseini, A. Advances in engineering hydrogels. *Science* **2017**, *356*, No. eaaf3627.

(2) Li, J.; Wu, S.; Kim, E.; Yan, K.; Liu, H.; Liu, C.; Dong, H.; Qu, X.; Shi, X.; Shen, J.; Bentley, W. E.; Payne, G. F. Electrobiofabrication: electrically based fabrication with biologically derived materials. *Biofabrication* **2019**, *11*, No. 032002.

(3) Yan, K.; Liu, Y.; Zhang, J.; Correa, S. O.; Shang, W.; Tsai, C.-C.; Bentley, W. E.; Shen, J.; Scarcelli, G.; Raub, C. B.; Shi, X.-W.; Payne, G. F. Electrical Programming of Soft Matter: Using Temporally Varying Electrical Inputs To Spatially Control Self Assembly. *Biomacromolecules* **2018**, *19*, 364–373.

(4) Servoli, E.; Maniglio, D.; Motta, A.; Migliaresi, C. Folding and Assembly of Fibroin Driven by an AC Electric Field: Effects on Film Properties. *Macromol. Biosci.* **2008**, *8*, 827–835.

(5) Yucel, T.; Kojic, N.; Leisk, G. G.; Lo, T. J.; Kaplan, D. L. Non-equilibrium silk fibroin adhesives. *J. Struct. Biol.* **2010**, *170*, 406–412.

(6) Kishore, V.; Paderi, J. E.; Akkus, A.; Smith, K. M.; Balachandran, D.; Beaudoin, S.; Panitch, A.; Akkus, O. Incorporation of a decorin biomimetic enhances the mechanical properties of electrochemically aligned collagen threads. *Acta Biomater.* **2011**, *7*, 2428–2436.

(7) Younesi, M.; Islam, A.; Kishore, V.; Panit, S.; Akkus, O. Fabrication of compositionally and topographically complex robust

tissue forms by 3D-electrochemical compaction of collagen. *Biofabrication* **2015**, *7*, No. 035001.
(8) Yi, H.; Wu, L.-Q.; Bentley, W. E.; Ghodssi, R.; Rubloff, G. W.; Culver, J. N.; Payne, G. F. Biofabrication with chitosan. *Biomacromolecules* **2005**, *6*, 2881−2894.
(9) Simchi, A.; Pishbin, F.; Boccaccini, A. R. Electrophoretic deposition of chitosan. *Mater. Lett.* **2009**, *63*, 2253−2256.
(10) Suginta, W.; Khunkaewla, P.; Schulte, A. Electrochemical biosensor applications of polysaccharides chitin and chitosan. *Chem. Rev.* **2013**, *113*, 5458−5479.
(11) Wu, S.; Yan, K.; Zhao, Y.; Tsai, C.-C.; Shen, J.; Bentley, W. E.; Chen, Y.; Deng, H.; Du, Y.; Payne, G. F.; Shi, X. Electrical writing onto a dynamically responsive polysaccharide medium: patterning structure and function into a reconfigurable medium. *Adv. Funct. Mater.* **2018**, *28*, No. 1803139.
(12) Anthonsen, M. W.; Smidsrød, O. Hydrogen ion titration of chitosans with varying degrees of N-acetylation by monitoring induced ^{1}H-NMR chemical shifts. *Carbohydr. Polym.* **1995**, *26*, 303−305.
(13) Sorlier, P.; Denuzière, A.; Viton, C.; Domard, A. Relation between the degree of acetylation and the electrostatic properties of chitin and chitosan. *Biomacromolecules* **2001**, *2*, 765−772.
(14) Morrow, B. H.; Payne, G. F.; Shen, J. pH-responsive self-assembly of polysaccharide through a rugged energy landscape. *J. Am. Chem. Soc.* **2015**, *137*, 13024−13030.
(15) Wu, L.-Q.; Gadre, A. P.; Yi, H.; Kastantin, M. J.; Rubloff, G. W.; Bentley, W. E.; Payne, G. F.; Ghodssi, R. Voltage-Dependent Assembly of the Polysaccharide Chitosan onto an Electrode Surface. *Langmuir* **2002**, *18*, 8620−8625.
(16) Liu, Y.; Kim, E.; Ghodssi, R.; Rubloff, G. W.; Culver, J. N.; Bentley, W. E.; Payne, G. F. Biofabrication to build the biology-device interface. *Biofarbication* **2010**, *2*, No. 022002.
(17) Cheng, Y.; Luo, X.; Betz, J.; Buckhout-White, S.; Bekdash, O.; Payne, G. F.; Bentley, W. E.; Rubloff, G. W. In situ quantitative visualization and characterization of chitosan electrodeposition with paired sidewall electrodes. *Soft Matter* **2010**, *6*, 3177−3183.
(18) Yan, K.; Ding, F.; Bentley, W. E.; Deng, H.; Du, Y.; Payne, G. F.; Shi, X.-W. Coding for hydrogel organization through signal guided self-assembly. *Soft Matter* **2014**, *10*, 465−469.
(19) Maki, Y.; Furusawa, K.; Yasuraoka, S.; Okamura, H.; Hosoya, N.; Sunaga, M.; Dobashi, T.; Sugimoto, Y.; Wakabayashi, K. Universality and specificity in molecular orientation in anisotropic gels prepared by diffusion method. *Carbohydr. Polym.* **2014**, *108*, 118−126.
(20) Liu, Y.; Zhang, B.; Gray, K. M.; Cheng, Y.; Kim, E.; Rubloff, G. W.; Bentley, W. E.; Wang, Q.; Payne, G. F. Electrodeposition of a weak polyelectrolyte hydrogel: remarkable effects of salt on kinetics, structure and properties. *Soft Matter* **2013**, *9*, 2703−2710.
(21) Lei, M.; Qu, X.; Liu, H.; Liu, Y.; Wang, S.; Wu, S.; Bentley, W. E.; Payne, G. F.; Liu, C. Programmable Electrofabrication of Porous Janus Films with Tunable Janus Balance for Anisotropic Cell Guidance and Tissue Regeneration. *Adv. Funct. Mater.* **2019**, *29*, No. 1900065.
(22) Netz, R. R. Nonequilibrium unfolding of polyelectrolyte condensates in electric fields. *Phys. Rev. Lett.* **2003**, *90*, No. 128104.
(23) Netz, R. R. Polyelectrolytes in electric fields. *J. Phys. Chem. B* **2003**, *107*, 8208−8217.
(24) Grass, K.; Holm, C. Polyelectrolytes in electric fields: measuring the dynamical effective charge and effective friction. *Soft Matter* **2009**, *5*, 2079−2092.
(25) Dewarrat, F.; Calame, M.; Schönenberger, C. Orientation and Positioning of DNA Molecules with an Electric Field Technique. *Single Mol.* **2002**, *3*, 189−193.
(26) Tang, J.; Du, N.; Doyle, P. S. Compression and self-entanglement of DNA molecules under uniform electric field. *Proc. Natl. Acad. Sci. U.S.A.* **2011**, *108*, 16153−16158.
(27) Lee, C.-H.; Hsieh, C.-C. Stretching DNA by electric field and flow field in microfluidic devices: An experimental validation to the devices designed with computer simulations. *Biomicrofluidics* **2013**, *7*, No. 014109.
(28) Zhou, C.; Reisner, W. W.; Staunton, R. J.; Ashan, A.; Austin, R. H.; Riehn, R. Collapse of DNA in AC Electric Fields. *Phys. Rev. Lett.* **2011**, *106*, No. 248103.
(29) Zhou, C.; Riehn, R. Collapse of DNA under alternating electric fields. *Phys. Rev. E* **2015**, *92*, No. 012714.
(30) Manghi, M.; Schlagberger, X.; Kim, Y.-W.; Netz, R. R. Hydrodynamic effects in driven soft matteri. *Soft Matter* **2006**, *2*, 653−668.
(31) Frank, S.; Winkler, R. G. Polyelectrolyte electrophoresis: Field effects and hydrodynamic interactions. *Europhys. Lett.* **2008**, *83*, No. 38004.
(32) O'Konski, C. T.; Zimm, B. H. New methods for studying electrical orientation and relaxation effects in aqueous colloids: preliminary results with tobacco mosaic virus. *Science* **1950**, *111*, 113−116.
(33) Kramer, H.; Deggelmann, M.; Graf, C.; Hagenbüchle, M.; Johner, C.; Weber, R. Electric Birefringence Measurements in Aqueous fd Virus Solutions. *Macromolecules* **1992**, *25*, 4325−4328.
(34) Jonsson, M.; Jacobsson, U.; Takahashi, M.; Nordén, B. Orientation of Large DNA during Free Solution Electrophoresis studied by Linear Dichroism. *J. Chem. Soc., Faraday Trans.* **1993**, *89*, 2791−2798.
(35) Schlagberger, X.; Netz, R. R. Orientation of elastic rods in homogeneous Stokes flow. *Europhys. Lett.* **2005**, *70*, 129−135.
(36) Boroudjerdi, H.; Kim, Y.-W.; Naji, A.; Netz, R.; Schlagberger, X.; Serr, A. Statics and dynamics of strongly charged soft matter. *Phys. Rep.* **2005**, *416*, 129−199.
(37) Oppermann, W. Transient electric birefringence of poly-(sodium p-styrenesulfonate) solutions at very low field strengths. *Makromol. Chem.* **1988**, *189*, 2125−2134.
(38) Tsai, C.-C.; Morrow, B. H.; Chen, W.; Payne, G. F.; Shen, J. Toward Understanding the Environmental Control of Hydrogel Film Properties: How Salt Modulates the Flexibility of Chitosan Chains. *Macromolecules* **2017**, *50*, 5946−5952.
(39) English, N. J.; Waldron, C. J. Perspectives on external electric fields in molecular simulation: progress, prospects and challenges. *Phys. Chem. Chem. Phys.* **2015**, *17*, 12407.
(40) della Valle, E.; Marracino, P.; Pakhomova, O.; Liberti, M.; Apollonio, F. Nanosecond pulsed electric signals can affect electrostatic environment of proteins below the threshold of conformational effects: The case study of SOD1 with a molecular simulation study. *PLoS One* **2019**, *14*, No. e0221685.
(41) Hoffmann, H.; Kramer, U.; Thurn, H. Anomalous Behavior of Micellar Solutions in Electric Birefringence Measurements. *J. Phys. Chem. A.* **1990**, *94*, 2027−2033.
(42) Yoshida, M.; Kikuchi, K.; Maekawa, T.; Watanabe, H. Electric Polarization of Rodlike Poly ions Investigated by Monte Carlo Simulations. *J. Phys. Chem. B.* **1992**, *96*, 2365−2371.
(43) Liu, Y.; Chakrabarti, B.; Saintillan, D.; Lindner, A.; du Roure, O. Morphological transitions of elastic filaments in shear flow. *Proc. Natl. Acad. Sci. U.S.A.* **2018**, *115*, 9438−9443.
(44) Plesa, C.; Verschueren, D.; Pud, S.; van der Torre, J.; Ruitenberg, J. W.; Witteveen, M. J.; Jonsson, M. P.; Grosberg, A. Y.; Rabin, Y.; Dekker, C. Direct observation of DNA knots using a solid-state nanopore. *Nat. Nanotechnol.* **2016**, *11*, 1093−1098.
(45) He, H.; Cao, X.; Dong, H.; Ma, T.; Payne, G. F. Reversible Programing of Soft Matter with Reconfigurable Mechanical Properties. *Adv. Funct. Mater.* **2017**, *27*, No. 1605665.
(46) Tsai, C.-C.; Payne, G. F.; Shen, J. Exploring pH-Responsive, Switchable Crosslinking Mechanisms for Programming Reconfigurable Hydrogels Based on Aminopolysaccharides. *Chem. Mater.* **2018**, *30*, 8597−8605.
(47) Hess, B.; Kutzner, C.; van der Spoel, D.; Lindahl, E. GROMACS 4: algorithms for highly efficient, load-balanced, and scalable molecular simulation. *J. Chem. Theory Comput.* **2008**, *4*, 435−447.

https://dx.doi.org/10.1021/acsomega.0c00164
ACS Omega 2020, 5, 12016−12026

(48) Guvench, O.; Greene, S. N.; Kamath, G.; Brady, J. W.; Venable, R. M.; Pastor, R. W.; MacKerell, A. D., Jr. Additive Empirical Force Field for Hexopyranose Monosaccharides. *J. Comput. Chem.* **2008**, *29*, 2543−2564.
(49) Guvench, O.; Hatcher, E.; Venable, R. M.; Pastor, R. W.; MacKerell, A. D., Jr. CHARMM Additive All-Atom Force Field for Glycosidic Linkages between Hexopyranoses. *J. Chem. Theory Comput.* **2009**, *5*, 2353−2370.
(50) Guvench, O.; Mallajosyula, S. S.; Raman, E. P.; Hatcher, E.; Vanommeslaeghe, K.; Foster, T. J.; Jamison, F. W., II; MacKerell, A. D., Jr. CHARMM additive all-atom force field for carbohydrate derivatives and its utility in polysaccharide and carbohydrate-protein modeling. *J. Chem. Theory Comput.* **2011**, *7*, 3162−3180.
(51) Brooks, B. R.; Brooks, C. L., III; Mackerell, A. D., Jr.; Nilsson, L.; Petrella, R. J.; Roux, B.; Won, Y.; Archontis, G.; Bartels, C.; Boresch, S.; Caflisch, A.; Caves, L.; Cui, Q.; Dinner, A. R.; Feig, M.; Fischer, S.; Gao, J.; Hodoscek, M.; Im, W.; Kuczera, K.; Lazaridis, T.; Ma, J.; Ovchinnikov, V.; Paci, E.; Pastor, R. W.; Post, C. B.; Pu, J. Z.; Schaefer, M.; Tidor, B.; Venable, R. M.; Woodcock, H. L.; Wu, X.; Yang, W.; York, D. M.; Karplus, M. CHARMM: the biomolecular simulation program. *J. Comput. Chem.* **2009**, *30*, 1545−1614.
(52) Hoover, W. G. Canonical dynamics: Equilibration phase-space distributions. *Phys. Rev. A* **1985**, *31*, 1695−1697.
(53) Parrinello, M.; Rahman, A. Polymorphic transitions in single crystals: A new molecular dynamics method. *J. Appl. Phys.* **1981**, *52*, 7182−7190.
(54) Hess, B.; Bekker, H.; Berendsen, H. J. C.; Fraaije, J. G. E. M. LINCS: A linear constraint solver for molecular simulations. *J. Comput. Chem.* **1997**, *18*, 1463−1472.
(55) Darden, T.; York, D.; Pedersen, L. Particle mesh Ewald: An N log(N) method for Ewald sums in large systems. *J. Chem. Phys.* **1993**, *98*, 10089−10092.

https://dx.doi.org/10.1021/acsomega.0c00164
ACS Omega 2020, 5, 12016−12026